THE JOURNAL OF PHYSICAL CHEMISTRY B

Article

pubs.acs.org/JPCB

Single Molecule Kinetics of ENTH Binding to Lipid Membranes

Sharon Rozovsky,*[,†] Martin B. Forstner,[‖] Holger Sondermann,[⊥] and Jay T. Groves*[,‡,§]

[†]Department of Chemistry and Biochemistry, University of Delaware, Newark, Delaware 19716, United States

[‖]Department of Physics, Syracuse University, Syracuse, New York 13210, United States

[⊥]College of Veterinary Medicine, Cornell University, Ithaca, New York 14853, United States

[‡]Howard Hughes Medical Institute, Department of Molecular and Cell Biology, University of California, Berkeley, Berkeley, California 94720, United States

[§]Physical Biosciences and Materials Sciences Divisions, Lawrence Berkeley National Laboratory, Berkeley, California 94720, United States

Supporting Information

ABSTRACT: Transient recruitment of proteins to membranes is a fundamental mechanism by which the cell exerts spatial and temporal control over proteins' localization and interactions. Thus, the specificity and the kinetics of peripheral proteins' membrane residence are an attribute of their function. Here, we describe the membrane interactions of the interfacial epsin N-terminal homology (ENTH) domain with its target lipid phosphatidylinositol (4,5)-bisphosphate (PtdIns(4,5)P_2). The direct visualization and quantification of interactions of single ENTH molecules with supported lipid bilayers is achieved using total internal reflection fluorescence microscopy (TIRFM) with a time resolution of 13 ms. This enables the recording of the kinetic behavior of ENTH interacting with membranes with physiologically relevant concentrations of PtdIns(4,5)P_2 despite the low effective binding affinity. Subsequent single fluorophore tracking permits us to build up distributions of residence times and to measure ENTH dissociation rates as a function of membrane composition. Furthermore, due to the high time resolution, we are able to resolve details of the motion of ENTH associated with a simple, homogeneous membrane. In this case ENTH's diffusive transport appears to be the result of at least three different diffusion processes.

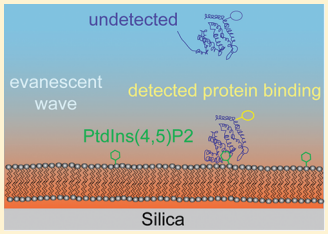

INTRODUCTION

Cellular membranes govern biochemical reactivity by controlling the associations of their affiliated proteins. A central mechanism is the dynamic membrane recruitment of peripheral membrane proteins, i.e., proteins that shuttle between lipidic and cytoplasmic locations. Following their attachment to the membrane, these proteins will encounter and interact with other proteins leading to key cellular processes such as endo- and exocytosis, cytoskeleton attachment, assembly of protein machineries, or restructuring of the membrane's shape.[1] For proper function, these processes rely on specific recognition and interaction of proteins with target membranes. This is often achieved by incorporating evolutionary conserved domains. Representative families of such structural motifs are the PH, PX, E/ANTH, PTB, FYVE, FERM, BAR, and PHD protein domains.[2] Individual proteins within each family share a common structural fold, lipid recognition elements, and related cellular functions. To alter the duration and spatial patterns of protein recruitment to membranes,[3,4] these domains typically bind phosphoinositides, signaling lipids whose phosphorylation and dephosphorylation are extensively used to regulate biochemical pathways. Because the specificity and affinity of membrane-targeting proteins to cellular membranes regulate their function, the residence time and diffusional transport of peripheral proteins on the membrane are directly correlated to their biological activity.

The focus of this study, the epsin N-terminal homology (ENTH) domain, is one of the better-characterized protein modules that employs an amphipathic helix for membrane integration.[5] Amphipathic helix insertion is one of the most commonly employed modes of membrane−protein associations and is used to tune the protein membrane residence all the way from transient to permanent attachment.[6−8] In general, amphipathic helices integrate parallel to the membrane surface where the helix polar residues contact the lipid headgroup while its nonpolar portion lie in the glycerol backbone region. The importance of amphipathic helices in recognizing and modifying the lipid environment has been increasingly appreciated in recent years.[9−11] The wealth of information regarding ENTH and its numerous, potential membrane association modes commends ENTH for a case study regarding the details of membrane interactions of peripheral membrane proteins.

ENTH itself is commonly found in proteins that mediate interactions with clathrin, ubiquitin, and other coat proteins.[12,13] Investigations of ENTH structure and function were previously conducted using a variety of experimental techniques.[8,14−18] In epsin (Eps15 interacting protein where

Received: October 19, 2011
Revised: February 27, 2012
Published: April 3, 2012

dx.doi.org/10.1021/jp210045r | J. Phys. Chem. B 2012, 116, 5122−5131

ENTH was originally identified[19]), binding of phosphatidylinositol (4,5)-bisphosphate (PtdIns(4,5)P_2) leads to the folding of an amphipathic helix from an unstructured N-terminal segment.[8] PtdIns(4,5)P_2 provides the majority of specific interactions between ENTH and lipids. However, the protein's affinity to membranes is further augmented by electrostatic attraction between clusters of basic residues and negatively charged lipids as well as integration of hydrophobic residues into the glycerol backbone−acyl chain interface.[17] Since the individual contributions of the different mechanisms can usually not be discerned, the complex interaction and binding process is often described using an average binding constant. However, it should be noted, that such binding affinities are only really valid for a particular membrane composition and the resulting surface charge scenario. In the case of highly charged membranes ENTH's effective binding affinity was found to be in the mid nanomolar range.[20]

In this study we focus on the binding affinity of ENTH to membranes at different charges and physiological concentrations of its target lipid, PtdIns(4,5)P_2. Imaging single molecules by total internal reflection fluorescence microscopy (TIRFM), we quantitatively measure properties of membrane association kinetics of the ENTH domain. Because in TIRFM only fluorophores within ∼100 nm of the interface are excited (Figure 1A) and thus imaged, this technique is particularly well suited to study interfacial interactions.[21] This was first clearly demonstrated by the pioneering studies of Thompson et al., where TRIFM was first employed to image directly protein−membrane interactions.[22−25] More recently, TIRFM was utilized to record binding events of individual PH membrane targeting domains.[26,27] These elegant measurements employing TIRFM demonstrated not only the ability to measure binding affinities of peripheral membrane proteins but also a careful examination of the effects of lipid binding stoichiometry.

Here, we measure the dissociation rate constant, diffusion rate, and details of ENTH diffusion when bound to the membrane by detecting the residence time and diffusion of ENTH to planar supported fluid lipid bilayer (SLB). Because we are able to achieve a time resolution of 13 ms, we can explore shorter residence times than previously possible, and thus we can record interactions of ENTH with weakly charged membranes. This ability to detect membrane associations of proteins with short residence times also enables us to use membranes with physiologically relevant concentrations of the target lipid PtdIns(4,5)P_2. Thus, we are able to resolve intricacies of the diffusive motion of membrane associated ENTH. It is found that lateral diffusion of ENTH along the membrane at these short time scales is best described by three different diffusion processes. Because this study utilizes simple, homogeneous lipid bilayers that are not known to form any membrane structures, the observed deviations from one component Brownian diffusion are most likely associated with different modes of interaction between ENTH and the membrane. The details of the diffusive behavior of peripheral membrane proteins are the foundation for understanding the search for target lipids or protein partners, which is essential for the formation of protein machineries. The high temporal resolution achieved in here enables the direct experimental observations necessary to test theoretical models and to understand interactions on the membrane's surface in quantitative terms.

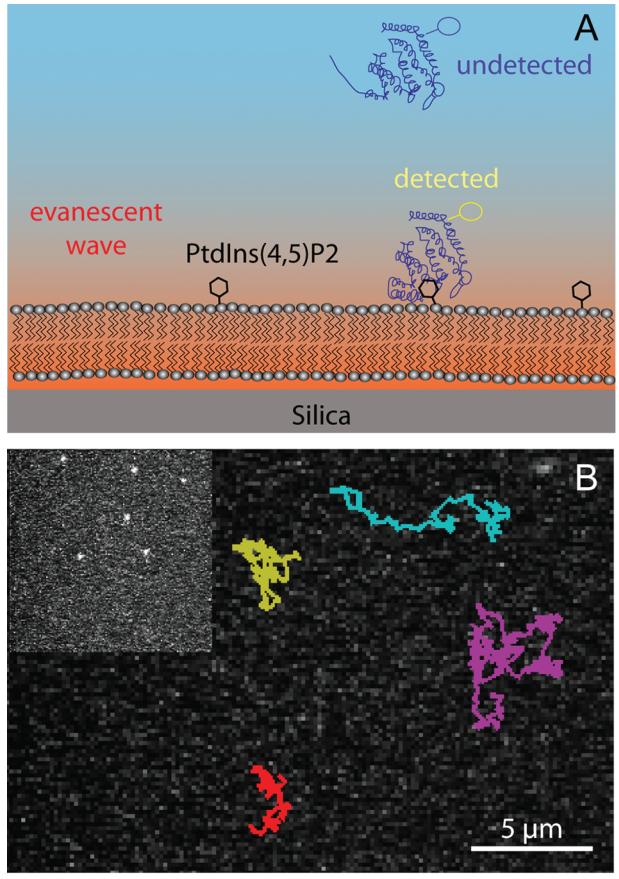

Figure 1. Imaging and tracking of individual ENTH proteins under TIRF illumination. (A) Visualization of the binding of individual ENTH proteins to a glass supported lipid bilayer containing its target lipid PtdIns(4,5)P_2 (green) by total internal reflection fluorescence microscopy. Fluorescently labeled proteins are in equilibrium between the solvent and a fluid lipid bilayer deposited on glass. A laser beam is total internally reflected at the glass−water interface creating a shallow illumination volume (orange) via the resulting evanescent wave. Within that volume, only membrane bound ENTH diffuses sufficiently slowly to be detected. (B) Trajectories (colored) of individual ENTH proteins diffusing on supported lipid bilayers (black background). Inset: original image showing the intensity of individual proteins.

MATERIALS AND METHODS

Materials. All reagents and solvents were at least analytical grade and were used as supplied. 1-Palmitoyl-2-oleoyl-*sn*-glycero-3-phosphocholine (POPC), 1-palmitoyl-2-oleoyl-*sn*-glycero-3-[phospho-L-serine] (POPS), and L-α-phosphatidylinositol-4,5-bisphosphate (Brain, Porcine) were from Avanti Polar Lipids (Alabaster, AL). Alexa Fluor 647 C2 maleimide and 1,1′-dioctadecyl-3,3,3′,3′-tetramethylindodicarbocyanine perchlorate (DiD) were supplied by Invitrogen (Carlsbad, CA). Enzymes used for molecular biology were acquired from New England Biolabs (Ipswich, MA). The chromatography media was supplied by GE Healthcare Bio-Sciences Corp. (Pittsburgh, PA) and Qiagen (Valencia, CA). All other chemicals and reagents were supplied by Sigma-Aldrich (St. Louis, MO).

Mutagenesis, Protein Expression, and Purification. ENTH domain (residues 1−164) from the human epsin 1 coding DNA (Open Biosystems Huntsville, AL) was cloned into the bacterial expression vector pProEx HTb (Invitrogen, Carlsbad, CA) using the *Bam*HI/XhoI cloning sites. Since the

dx.doi.org/10.1021/jp210045r | J. Phys. Chem. B 2012, 116, 5122−5131

native cysteine at position 96 is inaccessible for labeling, a Lys135Cys mutation was engineered using the QuikChange mutagenesis kit (Agilent, Santa Clara, CA) to introduce an exposed cysteine into the wild-type sequence (the resulting sequence is shown in Figure S5 of the Supporting Information). The plasmid was transformed into *Escherichia coli* BL21(DE3) cells (Novagen, San Diego, CA) for protein expression. Cells were grown in Terrific Broth at 37 °C, with good aeration and an ampicillin selection of 100 μg/mL. When the OD at 600 nm reached 0.7, the cells were incubated at 18 °C for an hour and protein expression was induced with 1 mM isopropyl-1-thio-β-D-galactopyranoside. The cell paste following a 16 h expression period was resuspended in 20 mM Tris-HCl, 500 mM NaCl, 20 mM imidiazole, 5 mM β-mercaptoethanol, pH 8.0 (NiNTA buffer), and lysed using a high-pressure homogenizer (EmulsiFlex-C5, Avestin, Ottawa, Canada). Cell debris was removed by ultracentrifugation at 100000*g* for 1 h. Clear supernatant was loaded onto a NiNTA column (Qiagen, Valencia, CA), and the protein was eluted using NINTA buffer supplemented with 500 mM imidiazole. The buffer was exchanged into 20 mM Tris-HCl (pH 8.0), 150 mM NaCl, 5 mM β-mercaptoethanol using a desalting column, and the His_6 tag was cleaved with tobacco etch virus (TEV) protease.[28] Following cleavage the protein N-terminal retained the sequence Gly-Pro-Met-Gly-Ser. The protein was passed over a NiNTA column at low imidiazole concentrations to remove the His_6-tagged TEV protease and uncleaved protein. The cleaved protein was further purified on a heparin column using a linear gradient of 150−1000 mM NaCl. Fractions containing pure ENTH were combined, concentrated, and further purified by size exclusion chromatography (HiPrep 16/60 Sephacryl S-100) in 20 mM Hepes (pH 7.4), 160 mM KCl, 10% glycerol. Protein purity, as determined by 15% SDS-PAGE gels, was at least 99%. The protein was concentrated to about 50 mg/mL, flash frozen in liquid N_2 and stored at −80 °C.

Fluorescent Labeling. Buffers were exchanged into 20 mM Hepes (pH 7.4), 160 mM KCl, 2 mM TCEP, 10% glycerol using a desalting column. The protein was reacted with the thiol reactive probe Alexa Fluor 647 C2 maleimide at a dye:protein ratio of 3:1 at 4 °C overnight. Then the reaction mixture was dialyzed extensively against 20 mM Hepes (pH 7.4), 160 mM KCl, 10% glycerol to remove the majority of the free dye. Residual free dye and protein aggregates were removed by size exclusion chromatography (HiPrep 16/60 Sephacryl S-100). The labeling efficiency was between 20% and 40% depending on the batch. The labeled protein was concentrated to about 30 mg/mL, flash frozen in liquid N_2, and stored at −80 °C. Within the measurement sensitivity flash frozen and freshly prepared ENTH behaved identically. ENTH showed no tendency to aggregate before or after freezing and storage.

Small Unilamellar Vesicles (SUVs) Preparation. Lipids were mixed in a chloroform/methanol solvent (2:1, lipids concentration 3 mg/mL); the solvent was evaporated with a rotary evaporator, dried under nitrogen, and desiccated for 12 h. Subsequently, the dried lipid film was hydrated in organic-free deionized (DI) water of high specific resistivity (~18.0 mΩ/cm) and left at room temperature for a few hours to swell. The vesicles were probe-sonicated in an ice−water bath utilizing a short duty cycle to avoid breakdown of phosphoinositides. Liposomes were centrifuged at 50000*g* for 2 h, and the upper supernatant fraction was retained. Liposomes were used within 2 days. Sonication was preferred over extrusion,[29] as we have found that the use of polycarbonate filters during extrusion increased significantly the level of fluorescent contaminations interfering with single molecule detection.

Samples. All measurements were conducted in a closed flow cell chamber (FCS2, Bioptechs, Butler, PA). To prepare for deposition of supported membranes, borosilicate glass cover slides with a diameter of 40 mm (Bioptechs, Butler, PA) were etched in piranha solution (3:1 H_2SO_4:H_2O_2). For the controls, silanized glass was prepared by first cleaning glass cover slides in piranha etch solution and then depositing 20 μL of octadecyltrimethoxysilicane between two dry glass cover slides. The assembly was incubated for 1 h at 80 °C. Once the surface was coated, excess material was rinsed in DI water. Silanized glass was used fresh immediately after preparation.

Glass-supported planar lipid bilayers were formed by incubation with SUVs solution (~0.4 mg/mL) in 20 mM Hepes, 160 mM KCl, pH 7.4. Excess of vesicles was washed away and AlexaFluor 647-labeled ENTH was injected to the chamber containing degassed and prefiltered buffer: 10 mM Hepes (pH 7.4), 160 KCl, and 2 mM trolox (6-hydroxy-2,5,7,8-tetramethylchroman-2-carboxylic acid). In addition to being a good triplet state quencher,[30] trolox is also a lipophilic antioxidant. All experiments utilized the above buffer and were carried out at room temperature (22 °C). Membrane integrity and fluidity were established by fluorescence recovery after photobleaching using DiD in membranes with identical compositions as those used in the single molecule measurements. SLBs was unaffected by the presence of the oxygen scavengers. While the use of blocking reagents is common in SLB-based experiments (typically a hydrophobic unstructured protein such as bovine serum albumin or casein), we found that in our application blocking was unhelpful. The quality of the supported lipid bilayer, as judged by the percent of static ENTH, presumably stuck to exposed glass, was in fact demised by the presence of blocking reagents. At our hand the single most important experimental factors that govern the bilayer quality are the etching process and the absence of any, even minute, osmotic shocks during preparation. By adopting the same buffer for all preparative steps—SLB formation, wash, and protein addition—the SLB integrity is uncompromised, and the number of defects is minimal. By optimizing SLB deposition conditions, it was possible to form an essentially defect free bilayer, as evident from the low number of static proteins. From the distribution of fluorophore intensities (Figure S2) it is clear that ENTH is a monomer while bound to and diffusing with the membrane. In fact, ENTH's free diffusion is the most direct and relevant validation of both its functionality and the integrity of the SLB membrane. SLB can often have microscopic defects that are not detected in bulk studies of SLB quality such as fluorescent recovery after photobleaching but are apparent in incubations of SLB and proteins by irreversible adhesion of proteins to exposed glass. In addition, control experiments were carried out with unlabeled ENTH under identical conditions to ensure that there are no contaminations in either the SLB or the protein.

Fluorophore Bleaching Rate. Because our experimental approach relays on signals from single fluorescent dyes, irreversible photobleaching could be a potential concern. For single molecule experiments the average lifetime of a fluorophore is often prolonged by the use of an oxygen scavenger system. Typically, these systems are an enzymatic mixture of glucose oxidase and catalase, which in the presence

of glucose turn free oxygen into hydrogen peroxide. We found that in our hands this oxygen scavenger system interfered with binding of ENTH to membranes. It is most likely that the produced hydrogen peroxide compromised either the protein and/or membrane integrity. However, the use of trolox as antifade agent[30] lead to prolonged fluorophore lifetimes without impacting ENTH−membrane interactions. Nevertheless, to ensure that photobleaching processes did not significantly bias our measurements of ENTH residence times and consequently the dissociation rate constant, we determined the bleaching rate of labeled ENTH immobilized on silanized glass. At conditions otherwise identical to the membrane experiments we measured a bleaching rate of 0.39 ± 0.08 s^{-1} (see right side of Figure 3) and an average fluorophore survival time before bleaching of 2.5 s. Because these values provide a comfortable measurement window compared to the time scales of ENTH membrane binding, we conclude that in our experiments the effect of photobleaching can to first order be neglected.

Total Internal Reflection Fluorescence Microscopy. Objective-type ("prismless") TIRFM experiments were preformed on an inverted microscope (TE2000, Nikon Corp., Tokyo, Japan) using a home-built system. A laser beam of 647 nm wavelength, generated by a water-cooled krypton/argon ion laser (Stabilite 2018 Spectra-Physics Lasers, Mounting View, CA), was enlarged via a Galilean beam expander (Optics for Research, Caldwell, NJ) and focused by a lens on the back-focal plane of a NA 1.45 PlanApo 100× oil immersion TIRF objective (Nikon Corp., Tokyo, Japan). Images were acquired with an EM-CCD-camera (Cascade II:512B, Photometrics, Tucson, AZ) using Metamorph image acquisition software (Universal Imaging Corp., Downingtown, PA).

Data Acquisition. Data were acquired with a 150 × 150 $pixels^2$ acquisition area (24.375 × 24.375 μm^2, total system resolution of 166.25 nm × 166.25 nm per pixel on the CCD) with a frame rate of 77 s^{-1}. Typically, 3000 frames were recorded per location. Particle statistics from about 20 films taken from different sample region were combined per condition. To avoid photobleaching or membrane heating, the microscope focus was adjusted prior to acquisition on a test region, and the stage was then moved to a new unperturbed location before images were acquired.

Simulated Image Sequences of 2D Random Walks. Simulated image sequences of single fluorophores diffusing in 2D were created by first generating random walks similar to the method described by Saxton.[31] A free 2D random walk can be decomposed into two independent one-dimensional walks in x and y directions. Thus, we simulate 2D diffusion by generating independent 1D random walks in each dimension. To that end, at every times step, δt, a step size, l, is picked from the step size probability distribution for a 1-dimensional random walk with diffusion coefficient, D, given by

$$p(l) = (2\pi D\delta t)^{-1} e^{-l^2/(2D\delta t)} \quad (1)$$

For each time step δt the distribution is inverted to calculate a step size based on a uniform random variable. We use a diffusion coefficient D = 1.5 $\mu m^2/s$ and δt = 13 ms (similar to the experimental observation and conditions). These random walks are then used as the basis of a simulated sequence of images. A simulated fluorophore was created with a Gaussian profile of the same width we observe via the camera in the real system and placed at every position of the random walk sequence. Finally, we added background noise at levels representative of real experiments. The generated movies were then analyzed using the algorithms described below.

Data Analysis. Particle tracking and data analysis were performed using custom software written in MatLab (The MathWorks, Natick, MA). The software integrates the IDL particle tracking software developed by Crocker and Grier[32] and converted to MatLab routines by Blair and Dufresne[33] and custom analysis procedures. In brief, images were filtered using a real-space bandpass filter, and particles were located by identifying a local brightness maxima followed by a 2D Gaussian or center of mass fit. 2D trajectories of individual proteins were constructed from the particle list by minimizing a probability distribution. The maximum displacement that a particle was allowed to move between frames and still be considered as the same particle was calculated from the 2D random walk root-mean-displacement assuming lipid diffusion in SLB is 3 × 10^{-12} m^2 s^{-1}.[34] The maximum displacement was set at two standard deviations.

Membrane bound ENTH freely diffuses. Thus, stationary proteins are attributed to binding to microscopic defects in the SLB that allows access to the glass. We define static particles as particles whose mean-squared displacement between frames during at least half of the trajectory length was lower than 0.8 $pixel^2$ (estimated empirically). Particles deemed static were automatically removed from the calculations. In addition, because short events could not be confidently distinguished from static proteins trajectories, we consider only trajectories longer than 3 time lags (~38 ms). In addition, trajectories that included positions within 8 pixels to the edge of the field of view were excluded. This is to avoid counting particles that left the camera field of view or were present at areas of uneven illumination compared to the rest of the sample.

Quantitative analysis of ENTH movement was based on routine MSD methods as previously described.[35] The two-dimensional MSD for each trajectory of ENTH was calculated according to the formula

$$\mathrm{MSD}(n\delta t) = \frac{1}{N-1-n}\sum_{j=1}^{N-1-n} \{[x(j\delta t + n\delta t) - x(j\delta t)]^2 + [y(j\delta t + n\delta t) - y(j\delta t)]^2\} \quad (2)$$

where δt is the time between frames, N is the total number of frames in a specific ENTH diffusion track, and n and j are positive integers specifying the time interval.

The distribution of diffusion coefficient for individual ENTH molecules was calculated as described by Saxton.[36] In brief, only protein trajectories that extended to t = 650 ms were selected and before further processing truncated to the same length. The individual step sizes of a given particle in 13 ms intervals were averaged and the diffusion coefficient calculated for that average ($D = \langle r \rangle/(4 \times 0.013\ s)$).

RESULTS AND DISCUSSION

In order to study the binding and unbinding of individual ENTH domains to membranes and to investigate their diffusion behavior in the absence of cells' complexity, a supported lipid bilayer (SLB) serves as *in vitro* membrane model. SLBs are commonly employed as biomimetic membrane systems because the lipid bilayers maintain their lateral mobility and their ability to accommodate and to adapt

to insertions of additional molecular components.[37] Hence, SLBs provide the adequate membrane environment required for maintaining function of peripheral membrane proteins. Creating the SLB on a thin glass slide permits the use of TIRF illumination. ENTH is labeled with a single fluorophore on a water-exposed location, and as illustrated in Figure 1A, TIRF's evanescent wave illuminates only ENTH near the membrane. Interactions of ENTH with PtdIns(4,5)P_2 containing membrane lead to its prolonged residence on the membrane within range of the TIRF illumination. The diffusion rate of the unbound ENTH is too fast (~100 $\mu m^2/s$)[38] to be detected under our experimental conditions, and only membrane bound proteins are thus detected. This allows imaging of membrane associated proteins with high signal-to-noise ratio (see inset in Figure 1B) at high temporal resolution (13 ms/frame). Information regarding ENTH's binding and diffusion behavior were extracted from the images by first determining the proteins' positions in each frame. This is achieved by fitting a Gaussian intensity profile as approximation of the fluorescent signal's point spread function. Judged by tracking of static ENTH immobilized on glass positional accuracy of about 10 nm was achieved. In the case of mobile ENTH (i.e., diffusing on SLBs) the positional accuracy is estimated to be closer to 50 nm.[39] These positions in each frame of the acquired image time series are then used to reconstitute the trajectories of individual proteins over time as shown in Figure 1B. These trajectories of single ENTH are the basis for our further analysis. We thereby extract the dissociation constant, k_{off}, as a function of PtdIns(4,5)P_2 concentration. Furthermore, the diffusion behavior of ENTH at the membrane is determined by calculation of the diffusion coefficients of individual proteins (an indication of their interactions with lipids), analysis of the step size distribution of the underlying random walks, and the distribution of individual diffusion coefficient in single fluorophore tracking experiments of finite track length. In the following we discuss these different observations and how they reflect on the ENTH binding process.

ENTH's Dissociation Rate. In order to quantitatively determine how membrane properties modulate the residence time of ENTH on the membrane, we measure the dissociation rate constant, k_{off}, as a function of membrane composition. The dissociation rate determines the time in which the concentration of the initially membrane bound proteins is reduced to half ($t_{1/2} = \ln(2)/k_{off}$). Therefore, it is a measure of a protein's tendency to reside on the membrane and along with the association rate it determines the protein's membrane binding affinity. Thus, for peripheral membrane proteins such as the ENTH domain, k_{off} is a key parameter that describes how long different proteins are available for productive encounters on the membrane.

Single molecule measurements are particularly well suited to determine the dissociation rate of peripheral membrane proteins, since the time an individual protein spends bound to the membrane can be directly observed. The distribution of these residence times of many individual molecules provides the probability that a protein will dissociate from the membrane after a certain time. Figure 2B illustrates this on a representative data set. For a simple unbinding process the surface dissociation rate, k_{off}, can be extracted from a fit of the experimentally obtained distribution of residence times to single exponential of the form $f(t) = A \exp(-t/k_{off})$. Because the residence times of many individual proteins are needed to reconstruct the distribution, k_{off} could be considered a bulk property in this case. However, the goodness of fit allows a direct assessment of the validity of the underlying binding model. Also, there are several additional advantages of this method compared to the common bulk techniques. First, the accessible binding regime is extended relatively to that typically available in bulk techniques (*vide infra*). Second, this method is flexible since it uses a simpler labeling scheme (e.g., no need for FRET pairs) than typical fluorescence based measurements. Third, the membrane state throughout the experiment can be monitored by determining the percent of immobile proteins, i.e., those that are bound to the membrane's defect sites (i.e., exposed glass).[40]

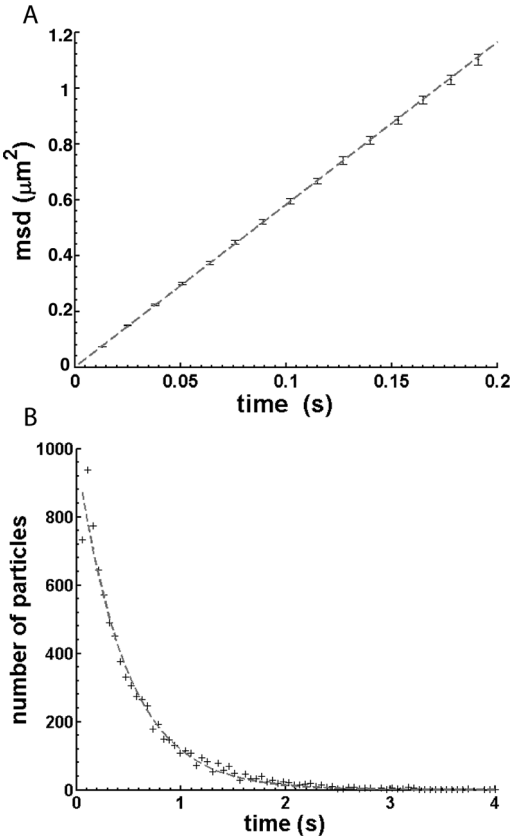

Figure 2. Analysis of a typical sample. (A) Time dependence of the mean-square displacement for ENTH diffusing on a SLB. For this sample ENTH diffusion coefficient is $D = 1.45 \pm 0.01$ $\mu m^2/s$. (B) A single-exponential fit to the distribution of ENTH residence times. The resulting k_{off} is 2.1 ± 0.1 s^{-1}. In this example, the SLB composition is 99 mol % POPC and 1 mol % PtdIns(4,5)P_2, the sample buffer is 20 mM Hepes, 160 mM KCl, 2 mM trolox, pH 7.4, and the concentration of the AlexaFluor 647-labeled ENTH in bulk solution is 1.6×10^{-13} M.

Using this approach, we determine the dependence of ENTH's dissociation rate constant on the membrane's PtdIns(4,5)P_2 content. As seen in Figure 3, ENTH's k_{off} is decreasing with increasing surface concentrations of the target lipid PtdIns(4,5)P_2. The dissociation rate constant for 2, 1, 0.5, and 0.1 mol % PtdIns(4,5)P_2 concentration was measured to be 4.5 ± 1.6, 6.8 ± 2.5, 12.5 ± 2.5, and 14 ± 6 s^{-1}, respectively. Assuming an average area per POPC of 0.7 nm^2,[41] these PtdIns(4,5)P_2 concentrations correspond approximately to 32000, 16000, 9000, and 1600 PtdIns(4,5)P_2 molecules per μm^2. Based on the crystal structure of ENTH, at the highest PtdIns(4,5)P_2 concentration the maximal coverage of the

dx.doi.org/10.1021/jp210045r | J. Phys. Chem. B 2012, 116, 5122–5131

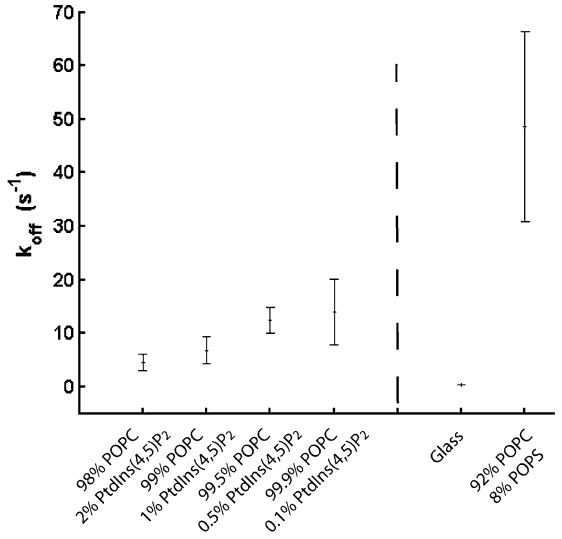

Figure 3. Dissociation rates of ENTH from bilayers with different compositions. Left of the dashed dividing line: ENTH dissociation rates from membranes of different composition. The residence time of the protein extends with increasing concentration of its target lipid due to increasing electrostatic attraction to the progressively more negatively charged surface as well as increasing frequency of rebinding processes. Data for each concentration were averaged from at least three independent measurements acquired on independent days with freshly prepared vesicles (the error bar is the standard deviation). Each value was averaged from at least 1000 particles. Right of the dividing line: ENTH dissociation rate from negatively charged bilayers with comparable charge to that of 99 mol % POPC and 1 mol % PtdIns(4,5)P_2. Also shown is the fluorophore lifetime when AlexaFluor 647-labeled ENTH is immobilized to silanized glass, indicating that the measured dissociation rates are not significantly influenced by photobleaching events.

membrane surface area by ENTH is at most 20%. In order to obtain the ideal number of distinct and distinguishable fluorescent signals, the ENTH concentrations in the buffer were adjusted for the different experiments to 1.6×10^{-13}, 3.2×10^{-13}, 8.1×10^{-13}, and 3.2×10^{-12} M, respectively. The error bars in Figure 3 reflect one standard deviation for experiments conducted with different vesicle preparation of identical compositions. However, deviations among experiment using the same vesicle preparation were less than 10%. This can readily be attributed to small variations in the PtdIns(4,5)P_2 concentrations between different separate vesicle preparations.

It is worthwhile to note that the measured effective k_{off} differ from previous bulk measurements using surface plasmon resonance (SPR) which yield a dissociation constant in the order of 3.0×10^{-2} s^{-1}.[16,20] This discrepancy originates most likely from fundamental differences between the experimental system of our study and that used in the SPR experiments. First, the solution concentrations of protein are by at least a factor of 1000 higher in the SPR experiments and a high surface coverage of bound ENTH in these experiments can be expected. In light of the work of Yoon et al.,[17] it seems likely that under these conditions ENTH has formed dimers and exhibit a significant lower dissociation rate due to the two binding sites per dimer. In our experiments, however, where the visualization of separate, single molecules necessitates very small protein concentrations, ENTH is most likely a monomer. A good experimental indicator of monomeric ENTH is given by the characteristic single step bleaching of the fluorescence signal of glass immobilized protein (see Figure S1 in the Supporting Information) as well as the unimodal intensity distribution of tracked objects (Figure S2). For several reasons, lipid packing and protein integration in our studies should be different, which in turn leads to additional differences in the dissociation constants. First, our study employs simple, homogeneous membranes composed of mostly POPC and a few mole percent PtdIns(4,5)P_2 while the SPR experiments contain up to 20 mol % POPE lipid. Second, small unilamellar vesicles are used in the SPR experiments while this study utilizes SLBs. Finally, there is a length difference of the N-terminal amphipathic helix of the ENTHs used in the different experiments.

To demonstrate the specificity of ENTH interactions with the target lipid, we performed experiments with membranes without PtdIns(4,5)P_2. In one set of experiments membranes were solely composed of the uncharged lipid POPC. We found that detectable encounters with the membrane were rare and so brief (~1−2 frame) that meaningful residence time distributions could not be constructed. However, we were able to detect nonspecific electrostatic attraction of ENTH to SLB by including the anionic lipid 1-palmitoyl-2-oleoyl-*sn*-glycero-3-phosphatidylserine (POPS) as negative surface charge carriers in the SLBs. As PtdIns(4,5)P_2 carries a net charge of approximately −4 at our solution conditions,[42] we mimicked the electrostatic properties of membranes containing 2 mol % PtdIns(4,5)P_2 by using lipid mixtures of 92 mol % POPC and 8 mol % POPS (ENTH solution concentration: 6.5×10^{-12} M). Significant interactions of ENTH with these membranes over several tens of milliseconds were detectable, resulting in a measured weak binding constant of 80 ± 6 s^{-1} (see right side of Figure 3). This value lies close to the 13 ms temporal detection limit of our TIRFM system as dictated by the time resolution of the EMCCD camera and our specific setup. Therefore, we did not attempt to further probe the binding behavior of ENTH on negatively charged bilayer. However, these experiments clearly demonstrate that ENTH has no significant interaction with uncharged lipid membranes, while electrostatic attraction—although the precise details are presently not well understood—should certainly play a role in recruiting ENTH to the membrane. With improved CCD camera resolution those details could be further investigated in the future to study the mechanisms that facilitate targeting and approach of peripheral membrane proteins to their binding partners.

ENTH's Lateral Diffusion and Average Diffusion Coefficient from Mean-Square Displacement Analysis. The diffusion of peripheral proteins and lipid-anchored proteins is influenced by the nature of the lipid−protein interface. Therefore, the diffusion coefficient contains mechanistic insight regarding protein attachment to the lipid bilayer, such as the number of lipids that interact and diffuse with the protein.[43,44] We recorded the tracks of individual ENTH due to 2D lateral diffusion of membrane bound protein as illustrated in Figure 3 (a typical sequence of images is available as movie M1 in the Supporting Information). Trajectories of individual ENTH proteins diffusing on the SLB were constructed from the proteins position in consecutive frames using a single particle tracking algorithms based on the work by Crocker and Grier.[32] The average ENTH diffusion coefficients, D, at different membrane compositions were derived from linear fits (weighted by the standard error of each point) to the mean-square displacement (MSD) as a function of time. For free 2D diffusion they are related by MSD = $4Dt$.[45] The representative

dx.doi.org/10.1021/jp210045r | J. Phys. Chem. B 2012, 116, 5122−5131

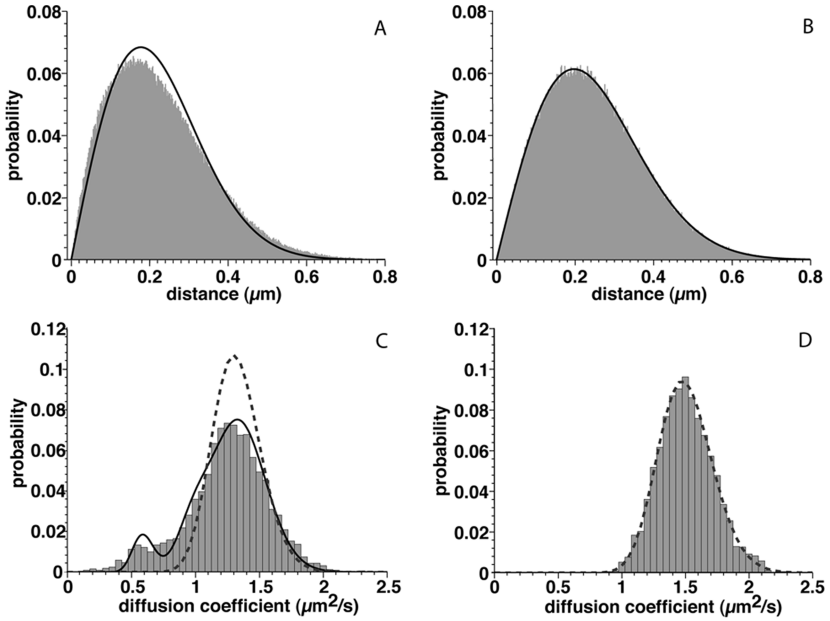

Figure 4. Analysis and comparison of simulated and experimental data. Top: step size distributions of ENTH diffusion on SLB calculated for steps taken during time interval of 13 ms (Δt = 13 ms). (A) Experimental data from ENTH diffusion on SLB composition is 99 mol % POPC and 1 mol % PtdIns(4,5)P_2. Overlaid (solid black line) is the best chi distribution fit to the step size distribution. The diffusion coefficient of the best fit is 1.2 $\mu m^2/s$, and that of the MSD fit is 1.5 $\mu m^2/s$. (B) Simulated data for a free 2D random walk. Both plots contain approximately 49000 individual steps. Bottom: histograms of the diffusion coefficient of all individual proteins whose residence time was at least 650 ms. (C) Experimental distribution from ENTH diffusion on SLB composition is 99 mol % POPC and 1 mol % PtdIns(4,5)P_2 (same sample analyzed in (A)). Overlaid (dotted gray line) on the experimental data (gray bars) is the best fit of the probability distribution of diffusion coefficients for Brownian walk using one average diffusion coefficient. The best fit, using three populations with different averaged diffusion coefficients, is overlaid (solid black line). (D) Simulated data for a free 2D random walk. Overlaid (dotted gray line) is the probability distribution of diffusion coefficients as calculated for a free 2D random walk using one average diffusion coefficient. The two distributions are reconstructed using 3200 individual particle tracks of 650 ms (50 frames).

MSD(t) plot in Figure 2A shows no significant deviations from a linear growth of the MSD with time. In addition, all diffusion coefficients determined this way lie within a narrow range between 1.2 and 1.5 $\mu m^2/s$, regardless of the PtdIns(4,5)P_2 concentration in the membrane. This indicates that at this level of analysis the diffusion behavior of membrane bound ENTH appears uniform and homogeneous. Diffusion coefficients of lipids in similar samples have been measured by fluorescence correlation spectroscopy (FCS) to be on the order of 3 $\mu m^2/s$,[46] consistent with other reported lipids' diffusion rates in SLBs. Considering the possibly substantial interactions of ENTH's amphipathic helix with the lipid bilayer, it is not surprising that ENTH's diffusion coefficient is about half of that of the lipids. A more detailed examination of diffusion coefficients of individual proteins is discussed in a later section.

Step Size Distribution. It is commonly assumed that membrane-binding proteins are capable of finding their ligands efficiently by electrostatically scanning of the surface.[47] In that case, ENTH should have at least two bound states: one loosely bound that is due to unspecific electrostatics and one PtdIns(4,5)P_2-bound that should be tighter. This difference in association should lead to differences in the diffusive behavior of the protein. In order to evaluate whether the motion of membrane associated ENTH exhibits deviations from a free two-dimensional random walk with one diffusion coefficient, we examined the distribution of step sizes (i.e., the distance traveled) in a given time interval. The step size distribution of a 2D diffusion process resulting from a random walk is described by a chi distribution.[48] The probability that a particle diffused a net distance r during a time Δt is given by

$$P(r, \Delta t) = \frac{r}{2D\Delta t} \exp\left(\frac{-r^2}{4D\Delta t}\right) \quad (3)$$

where D is the diffusion coefficient. This behavior has also been observed experimentally for Brownian diffusion of lipids in pure lipid bilayers.[49] The step size distribution of a more complex diffusion or binding process will generally deviate from such a chi distribution.

In Figure 4A, a representative distribution of step sizes of membrane bound ENTH during a time interval Δt = 13 ms is shown. The black line overlaid on the histogram is the corresponding chi distribution using the best fit. Clearly visible is the deviation of the experimental step size distribution from the expected chi distribution based on the measured diffusion coefficient. The large number of steps (>45000) used to construct the histogram argues against an undersampled distribution. In order to rule out that this deviation is caused by imaging artifacts[49] or biases in the tracking algorithm, we employed simulated images based on 2D random walks with a diffusion coefficient of 1.5 $\mu m^2/s$. At each position of the walk we placed the intensity profile of a single fluorophore and added Gaussian noise at a level of the average experiment. The resulting histogram of step sizes of such a simulation using the same number of steps is plotted in Figure 4B. Now the black curve—again representing the chi distribution—is a very good fit to this histogram. This shows that the deviation at short steps observed in the experiments is a most likely a real feature and not an artifact.

To further solidify the deviation of membrane bound ENTH from Brownian diffusion with a single diffusion coefficient, we calculated the diffusion coefficients of individual proteins and

dx.doi.org/10.1021/jp210045r | J. Phys. Chem. B 2012, 116, 5122–5131

investigated their distribution. This distribution of diffusion coefficients in single molecule tracks of a given length is given by[36]

$$p(D)\,\mathrm{d}D_e = \frac{1}{(N-1)!}\left(\frac{N}{D_0}\right)^N D_e^{N-1}\exp\left(\frac{-ND_e}{D_0}\right)\mathrm{d}D_e \quad (4)$$

where N is the number of frames, D_0 is the true mean diffusion coefficient, and D_e is the experimental diffusion coefficient for an individual trajectory. The histogram of close to 3200 individual diffusion coefficients taken from a representative data set is shown in Figure 4C. D_e of individual proteins was calculated for all tracks that exceeded $t = 0.65$ s by analyzing the first 50 frames of the particle's trajectory. The individual steps taken by the same particle per time delay are averaged and calculated according to $D_e = r^2/4\delta t$ where δt = 13 ms. The resulting histogram of diffusion coefficients from single tracks is plotted in Figure 4C. The dashed line represents the fit using eq 4 (using $D_e = 1.3\ \mu m^2/s$) and clearly demonstrates that the observed data are not well described by a single 2D diffusion process. However, we obtained the best fit by assuming that ENTH can undergo three different diffusion processes at the membrane. A linear combination of the expression above gives the fit plotted as a solid black line in Figure 4C. (The resulting diffusion coefficients and corresponding weights are $D_{e1} = 1.14\ \mu m^2/s$ with a weight of 0.695, $D_{e2} = 1.04\ \mu m^2/s$ with a weight of 0.220, and $D_{e3} = 0.66\ \mu m^2/s$ with a weight of 0.085.) Similar to the case of the step size distribution, we used simulated images to validate out tracking and analysis algorithms. As seen in Figure 4D, the random walk described by one diffusion coefficient is well fitted by the analytical expression of eq 4. Again, this strongly suggests that the observed deviation from one component Brownian diffusion is indeed a real feature of the experimental system. The observed deviation can in general have several underlying causes. However, most of them can be ruled out in this case. As described above, dimer formation in this system is unlikely, which rules out protein−protein interactions and subsequent membrane remodeling as source for complex diffusion behavior as seen for example in the work by the Gai group.[50,51] Also, complex membrane structures such as lipid micro domains can be ruled out because the used membrane system of mostly POPC and a few mol % of PtdIns(4,5)P_2 is not known to exhibit any inherent structures but provides for a simple and homogeneous lipid bilayer. Furthermore, Ca^{2+}-induced PtdIns(4,5)P_2 clusters[52,53] are unlikely due to the absence of Ca^{2+} ions in the used buffer system. Finally, anomalous diffusion may be considered. However, the step size and diffusion coefficient distributions for lager time scales (Figures S3 and S4 in the Supporting Information) reveal that at longer times the details of the underlying distributions disappear, and a single component Brownian diffusion process emerges. This observation indicates that the central limit theorem is valid in this situation, which in turn rules out anomalous diffusion. Thus, the observed, multiple diffusion processes at short times should be due solely to the interaction of ENTH with the membrane.

CONCLUSIONS

Here, we report measurements of the kinetic binding of the peripheral membrane protein ENTH to lipid bilayers at physiological concentration of the protein's target lipid PtdIns(4,5)P_2. Determination of the effective dissociation rate of ENTH from the membrane based on single molecule trajectories was thereby relatively straightforward. The experimentally observed diffusion behavior of membrane associated ENTH, however, seems on a first glance surprising.

The growth with time of the MSD determined from the tracks of the protein diffusing on the lipid bilayer seems to follow a linear relationship as expected from a single component Brownian diffusion process. However, a closer examination of the step size distributions and the distribution of diffusion coefficients of individual proteins clearly show that the mode of transport of membrane associated ENTH is not diffusion described by one diffusion coefficient. The distributions suggest that ENTH can have more than one diffusional process at the membrane. It is well documented that specific interactions of proteins and biomembranes *in vivo* can cause complex diffusion behavior.[54] Yet, here we see a clear experimental evidence for such complex diffusion behavior in a very simple membrane system, i.e., in the absence of the complex supramolecular structure of cellular biomembranes. We attribute this behavior to different diffusive behavior of ENTH before encountering the target lipid, PtdIns(4,5)P_2, and while bound to it. ENTH, whose crystal structure demonstrates a patch of positive charges on its surface, is electrostatically attracted to the negatively charged bilayer. Upon encountering and binding its target lipid, PtdIns(4,5)P_2, ENTH undergoes a conformational change where the unstructured N-terminus forms an amphipathic helix, the hydrophobic part of which intercalates into the leaflet.[17] These different bound states are likely to have different structural conformations with different degrees of desolvation of the membrane interface. They are likely to have different binding affinity and different diffusion rates since the number of associated lipids will vary.

Nonspecific electrostatic attraction of cellular components to membranes is a general mechanism for concentrating reactive chemical species and macromolecules by the membrane and increasing the likelihood of finding and binding a lipid/protein partner. The screening capacity of proteins to probe the membrane surface in search of their target has important physicochemical consequences, and as such its quantitative description is essential for description of interfacial behavior.[47,55,56] While this view of the search process is well-established, direct experimental validation has proven to be challenging due to the time scale of the interactions and the inability to distinguish between different protein populations in bulk. Recently, single molecule TIRFM detection has provided direct observations that electrostatic interactions are key to orientating the protein in relation to the membrane and facilitating binding of rare target lipids.[26] The temporal resolution of our single molecule experiments described in here provide direct evidence for several diffusional processes that mirror the complex interactions between protein's and their target membranes.

Given this signature of complex interactions between ENTH and the membrane, future efforts should strive to conclusively associate the observed diffusive processes with particular protein conformations and the resulting interactions with both PtdIns(4,5)P_2 and the membrane as a whole. Thus, the logical extension of this work is experiments in which also the target lipid as well as the conformational state of the protein can be observed simultaneously. Such measurements would provide further insight in the interplay between configurational states of the protein and membrane properties. This valuable information would be essential in understanding the kinetics

and energetics of assembling protein machineries at the membrane surface.

In conclusion, we demonstrate in here quantitative measurements of membrane association kinetics of peripheral membrane proteins with low membrane binding affinity which is frequently exhibit by peripheral membrane proteins. In addition, we show that measurements of interactions of proteins with membranes containing a small—and therefore physiologically relevant—amount of the target lipid are feasible. Finally, we present clear evidence for complex diffusive behavior of membrane-associated ENTH that indicates at least three different diffusive processes.

■ ASSOCIATED CONTENT

Supporting Information

Movie M1 provides an example of a typical image sequence; Figure 1S presents stepwise bleaching characteristics, and Figure 2S shows the distribution of intensities in order to demonstrate ENTH is a monomer in our measurements; Figure 3S contains distributions of individual diffusion coefficients for different time intervals between steps; Figure 4S shows distributions of step sizes for different time intervals; Figure 5S provides the amino acid sequence of the ENTH protein used in our study. This material is available free of charge via the Internet at http://pubs.acs.org.

■ AUTHOR INFORMATION

Corresponding Author

*E-mail: JTGroves@lbl.gov (J.T.G.); rozovsky@udel.edu (S.R.).

Notes

The authors declare no competing financial interest.

■ ACKNOWLEDGMENTS

The authors thank Dr. John Kuriyan and his group members for their expert advice and use of lab facilities and Dr. Daniel Blair, Dr. Andy Demond, and Dr. Nathan Clack for sharing computer code. We also thank Dr. Mahendra Jain, Dr. Sophie Pautot, and Neil Switz for insightful discussions. This work was supported by the Director, Office of Science, Office of Basic Energy Sciences, Chemical Sciences, Geosciences, and Biosciences Division of the U.S. Department of Energy (DOE) under Contract DE-AC02-05CH11231.

■ REFERENCES

(1) Lemmon, M. A. *Nat. Rev. Mol. Cell Biol.* **2008**, *9*, 99.
(2) Cho, W. H.; Stahelin, R. V. *Annu. Rev. Biophys. Biomol. Struct.* **2005**, *34*, 119.
(3) Roth, M. G. *Physiol. Rev.* **2004**, *84*, 699.
(4) Di Paolo, G.; De Camilli, P. *Nature* **2006**, *443*, 651.
(5) De Camilli, P.; Chen, H.; Hyman, J.; Panepucci, E.; Bateman, A.; Brunger, A. T. *FEBS Lett.* **2002**, *513*, 11.
(6) Cornell, R. B.; Taneva, S. G. *Curr. Protein Pept. Sci.* **2006**, *7*, 539.
(7) White, S. H.; Ladokhin, A. S.; Jayasinghe, S.; Hristova, K. *J. Biol. Chem.* **2001**, *276*, 32395.
(8) Ford, M. G. J.; Mills, I. G.; Peter, B. J.; Vallis, Y.; Praefcke, G. J. K.; Evans, P. R.; McMahon, H. T. *Nature* **2002**, *419*, 361.
(9) Drin, G.; Antonny, B. *FEBS Lett.* **2010**, *584*, 1840.
(10) Shibata, Y.; Hu, J. J.; Kozlov, M. M.; Rapoport, T. A. *Annu. Rev. Cell Dev. Biol.* **2009**, *25*, 329.
(11) Zimmerberg, J.; Kozlov, M. M. *Nat. Rev. Mol. Cell Biol.* **2006**, *7*, 9.
(12) Maldonado-Baez, L.; Wendland, B. *Trends Cell Biol.* **2006**, *16*, 505.
(13) Coon, B. G.; Burgner, J.; Camonis, J. H.; Aguilar, R. C. *J. Biol. Chem.* **2010**, *285*, 33073.
(14) Itoh, T.; Koshiba, S.; Kigawa, T.; Kikuchi, A.; Yokoyama, S.; Takenawa, T. *Science* **2001**, *291*, 1047.
(15) Ford, M. G. J.; Pearse, B. M. F.; Higgins, M. K.; Vallis, Y.; Owen, D. J.; Gibson, A.; Hopkins, C. R.; Evans, P. R.; McMahon, H. T. *Science* **2001**, *291*, 1051.
(16) Stahelin, R. V.; Long, F.; Peter, B. J.; Murray, D.; De Camilli, P.; McMahon, H. T.; Cho, W. *J. Biol. Chem.* **2003**, *278*, 28993.
(17) Yoon, Y.; Tong, J.; Lee, P. J.; Albanese, A.; Bhardwaj, N.; Kaellberg, M.; Digman, M. A.; Lu, H.; Gratton, E.; Shin, Y.-K.; Cho, W. *J. Biol. Chem.* **2010**, *285*, 531.
(18) Friant, S.; Pecheur, E. I.; Eugster, A.; Michel, F.; Lefkir, Y.; Nourrisson, D.; Letourneur, F. *Dev. Cell* **2003**, *5*, 499.
(19) Chen, H.; Fre, S.; Slepnev, V. I.; Capua, M. R.; Takei, K.; Butler, M. H.; Di Fiore, P. P.; De Camilli, P. *Nature* **1998**, *394*, 793.
(20) Hom, R. A.; Vora, M.; Regner, M.; Subach, O. M.; Cho, W.; Verkhusha, V. V.; Stahelin, R. V.; Kutateladze, T. G. *J. Mol. Biol.* **2007**, *373*, 412.
(21) Axelrod, D. *Methods Enzymol.* **2003**, *361*, 1.
(22) Lagerholm, B. C.; Starr, T. E.; Volovyk, Z. N.; Thompson, N. L. *Biochemistry* **2000**, *39*, 2042.
(23) Lagerholm, B. C.; Thompson, N. L. *Biophys. J.* **1998**, *74*, 1215.
(24) Lagerholm, B. C.; Thompson, N. L. *J. Phys. Chem. B* **2000**, *104*, 863.
(25) Lieto, A. M.; Cush, R. C.; Thompson, N. L. *Biophys. J.* **2003**, *85*, 3294.
(26) Knight, J. D.; Falke, J. J. *Biophys. J.* **2009**, *96*, 566.
(27) Knight, J. D.; Lerner, M. G.; Marcano-Velazquez, J. G.; Pastor, R. W.; Falke, J. J. *Biophys. J.* **2010**, *99*, 2879.
(28) Kapust, R. B.; Tozser, J.; Fox, J. D.; Anderson, D. E.; Cherry, S.; Copeland, T. D.; Waugh, D. S. *Protein Eng.* **2001**, *14*, 993.
(29) Mui, B.; Chow, L.; Hope, M. J. *Methods Enzymol.* **2003**, *367*, 3.
(30) Rasnik, I.; McKinney, S. A.; Ha, T. *Nat. Methods* **2006**, *3*, 891.
(31) Saxton, M. J. *Biophys. J.* **1993**, *64*, 1766.
(32) Crocker, J. C.; Grier, D. G. *J. Colloid Interface Sci.* **1996**, *179*, 298.
(33) http://physics.georgetown.edu/matlab/.
(34) Tocanne, J. F.; Dupoucezanne, L.; Lopez, A. *Prog. Lipid Res.* **1994**, *33*, 203.
(35) Gross, D. J.; Webb, D. D. In *Spectroscopic Membrane Probes II*; Loew, L. M., Ed.; CRC Press: Boca Raton, FL, 1988; p 19.
(36) Saxton, M. J. *Biophys. J.* **1997**, *72*, 1744.
(37) Tamm, L. K.; McConnell, H. M. *Biophys. J.* **1985**, *47*, 105.
(38) Luby-Phelps, K. *Int. Rev. Cytol.* **2000**, *192*, 189.
(39) Sharonov, A.; Bandichhor, R.; Burgess, K.; Petrescu, A. D.; Schroeder, F.; Kier, A. B.; Hochstrasser, R. M. *Langmuir* **2008**, *24*, 844.
(40) Sackmann, E. *Science* **1996**, *271*, 43.
(41) Wenzl, P.; Fringeli, M.; Goette, J.; Fringeli, U. P. *Langmuir* **1994**, *10*, 4253.
(42) McLaughlin, S.; Wang, J. Y.; Gambhir, A.; Murray, D. *Annu. Rev. Biophys. Biomol. Struct.* **2002**, *31*, 151.
(43) Zhang, L. F.; Granick, S. *Proc. Natl. Acad. Sci. U. S. A.* **2005**, *102*, 9118.
(44) Saffman, P. G.; Delbruck, M. *Proc. Natl. Acad. Sci. U. S. A.* **1975**, *72*, 3111.
(45) Einstein, A. *Ann. Phys. (Berlin, Ger.)* **1905**, *15*, 549.
(46) Paulick, M. G.; Wise, A. R.; Forstner, M. B.; Groves, J. T.; Bertozzi, C. R. *J. Am. Chem. Soc.* **2007**, *129*, 11543.
(47) Adam, G.; Delbruck, M. In *Structural Chemistry and Molecular Biology*; Rich, A., Davidson, N., Eds.; W.H. Freeman and Company: San Francisco, 1968.
(48) Chandrasekhar, S. *Rev. Mod. Phy.* **1943**, *15*, 0001.
(49) Martin, D. S.; Forstner, M. B.; Kas, J. A. *Biophys. J.* **2002**, *83*, 2109.
(50) Smith-Dupont, K. B.; Guo, L.; Gai, F. *Biochemistry* **2010**, *49*, 4672.
(51) Guo, L.; Smith-Dupont, K. B.; Gai, F. *Biochemistry* **2011**, *50*, 2291.

(52) Ellenbroek, W. G.; Wang, Y. H.; Christian, D. A.; Discher, D. E.; Janmey, P. A.; Liu, A. J. *Biophys. J.* **2011**, *101*, 2178.
(53) Levental, I.; Christian, D. A.; Wang, Y. H.; Madara, J. J.; Discher, D. E.; Janmey, P. A. *Biochemistry* **2009**, *48*, 8241.
(54) Dix, J. A.; Verkman, A. S. *Annu. Rev. Biophys.* **2008**, *37*, 247.
(55) Axelrod, D.; Wang, M. D. *Biophys. J.* **1994**, *66*, 588.
(56) Delisi, C. *Q. Rev. Biophys.* **1980**, *13*, 201.